สำนักงานวิทยทรัพยากร
จุฬาลงกรณ์มหาวิทยาลัย

CHAPTER IV

Transient and Steady State Deformations of Dispersed –Phase Droplets of Immiscible Polymer Blends in Steady State Shear Flow

Abstract

Transient and steady state deformations and breakup of viscoelastic polystyrene (PS) droplets dispersed in viscoelastic high density polyethylene (HDPE) matrix were observed under a simple steady state shearing flow between two transparent parallel disks. The influences of elasticity of the blend constituent components, the matrix shear force, and the viscosity ratio on the transient deformation, the droplet steady state size, and the breakup sequence were investigated. After the startup of a steady state shearing flow, the viscoelastic droplet shape initially shows small oscillations in the flow direction, and eventually oscillates and deforms in the vorticity direction. The steady-state deformation of droplet along the vorticity direction decreases with increasing capillary number, viscosity ratio and the droplet elaticity.. When the critial capillary number, Ca_c, was exceeded, the droplet stretches and forms a string which becomes thinner and finally break up along the vorticity direction, provided that the droplet elasticity is sufficiently high. When the matrix shear force and the droplet elaticity are kept constant, the steady-state deformation along the vorticity direction and the critical capillary number for breakup are found to increase with the viscosity ratio varying from 0.5 to 1.0, and to 2.6.

I. INTRODUCTION

The fundamental understanding of ther deformed droplet shape is based on the work of Taylor (1932)[1] and (1934)[2], who found the two dimensionless parameters that control the droplet behavior under shear flow. The first parameter is the viscosity ratio between the two phases;

$$\eta_r = \eta_d / \eta_m \qquad (1)$$

where η_d and η_m are the viscosities of the droplet and the matrix phases, respectively. The second dimensionless parameter is the Capillary number

$$Ca = \frac{D_0 \dot{\gamma} \eta_m}{2\Gamma} \qquad (2)$$

where $\dot{\gamma}$ is the shear rate, D_0 is initial droplet diameter, and Γ is the interfacial tension. Taylor (1932,1934) found that deformation parameter, Def, depending on Ca and η_r is given by

$$Def \equiv \frac{a-b}{a+b} = Ca \frac{19\eta_r + 16}{16\eta_r + 16} \qquad (3)$$

where a and b are lengths of the major and minor axes of the deformed droplet, respectively. The capillary number is a measure of the ratio between the viscous stress and the interfacial stress. There exists a critical capillary number, Ca_c, which determines the stability of a droplet in a flow field.

Vassilios et al.[3] studied deformation and breakup machanisms of single drops during shear of isotropic hydroxypropylcellulose immersed in a polydimethylsiloxane matrix by using a rheo-optical technique. The nonstationary deformation and breakup mechanisms of drops were characterized at large capillary number. The deformation of threads followed a pseudo affine deformation for Ca/Ca_c larger than 2.5 and above a certain strain. They reported that the thread rupture results from a competition between end pinching and capillary instability mechanisms. The end pinching mechanism occurred at a specific scaled strain, which included the initial drop size and the applied shear rate. Capillary instabilities developed when the thread diameter reached a critical value inversely proportional to

หอสมุดกลาง สำนักงานวิทยทรัพยากร
จุฬาลงกรณ์มหาวิทยาลัย

the applied shear rate. The time necessary for the total rupture of a thread depended on the initial drop diameter, the applied shear rate, and the critical thread diameter or the applied shear rate which can influence on the time necessary for breakup. Jong-Wook and Gary Leal[4] studied drop deformation and breakup in extensional flow at high capillary number for blends of Newtonian drops in a suspending fluid, and study of Newtonian drops in a viscoelastic suspending fluid. They found that the critical degree of stretch for breakup increases sharply with the increase of the capillary number that characterizes the stretching process for Newtonian drops in a Newtonian suspending fluids. Newtonian drops in the viscoelastic boger fluid were found to be slightly more stable than the same drops in a Newtonian fluid when stretched at strain rates just exceeding the critical value. The critical elongation ratio necessary for the drops to break upon cessation of flow was increased by about 20 %, approximately 2.15 times the critical value. Large drops in the viscoelastic fluid were destabilized in a Newtonian suspending fluid, while smaller drops were strongly stabilized. For simple shear flow, the shape of the curve Ca_c vs η_r is well known; for $\eta_r \approx 1$ it has a minimum at $Ca_c \cong 0.5$ (Taylor 1932,1934)[1,2], for $\eta_r > 4$ it becomes infinite so that droplets are stable at all capillary numbers [Grace][5] . Tavgac[6], studied the deformation and breakup of viscoelastic drops suspended in a viscoelastic fluid under shear flow. He observed that, depending on drop/matrix combined properties, the elastic forces arising from the droplet phase may have a stabilizing or destabilizing effect on the breakup process. At high values of viscosity ratio, an elastic droplet unfavored the breakup, but destabilized the drops at low values of viscosity ratio and he also reported that the breakup of viscoelastic drops in viscoelastic matrices occurred at lower shear rates under transient conditions compared to steady-state conditions. These results strongly suggest that droplet deformation and breakup are strongly influenced by viscosity ratio.

However, it is well know that polymeric blends do not follow the simple behaviors predicted by the Taylor theory. F. Mighri et al.[7] studied the effect of elasticity on drop deformation in elongational flow driven through a transparent channel of plexiglasses with a converging and diverging cross sectional channel They found that the drop deformation decreased with increasing drop elasticity. On

the other hand, the matrix elasticity had the opposite effect. They defined the elasticity ratio, K', as the ratio of the maxwell relaxation time (λ) of the drop phase to that of the matrix phase, where $\lambda = N_1/ 2\eta\gamma^2$. They reported that for K' < 0.2, the matrix elasticity had more effect on the drop deformation than the drop elasticity. However, for K' > 0.2 the drop deformation was more affected by the drop elasticity. Mighri et al.[8] investigated the influence of elastic properties on the drop deformation and breakup in shear flow. The matrix phase was prepared from 92 % maltose syrup with various amounts of distilled water (7.9-8.0%) and varying PAA (0.0-0.1%). The drop fluids were prepared from 93 % PB with various amounts of kerosene (6.2-8.4 %) and PIB (0.0-1.2 %). The experiments were conducted by using two transparent parallel disks mounted on a R-18 Weissenberg rheogoniometer . They found that the matrix elasticity helped to deform the drop whereas the drop elasticity resisted the drop deformation. Breakup increased with increasing drop/matrix elasticity ratio, K'. For the matrix of high elasticity (K' < 0.37), the deformation of elastic drops in an elastic matrix under shear was higher than that of Newtonian drops in a Newtonian matrix at the same viscosity ratio and interfacial tension. However, for K' > 0.37 the elastic drops deformed less than a Newtonian drop in a Newtonian matrix. Moreover, they proposed that the critical shear rate and breakup time increased with increasing elasticity ratio; for K' < 4 the critical capillary number increased rapidly with rising K' and for K' > 4 it achieved a maximum of about 1.75. Lerdwijitjarud et al.[9] studied blends of polystyrene drop and high density polyethylene at fixed viscosity ratios of 0.5, 1, and 2 by using a cone and plate rheometer. They proposed that after steady-state shearing, the viscoelastic drops were larger than the Newtonian drops at the same shearing stress and the value of steady-state capillary number increased with the first normal stress difference ratio and it followed a power law with scaling exponents between 1.7 and 1.9. Lerdwijitjarud et al.[10] reported that for blends of polybutadiene in poly(dimethylsiloxane), both isolated droplets and 20% dispersed phase blend were investigated under conditions of equal viscosities of droplet and matrix fluids. They found that the droplet-phase elasticity increased, the steady-state shape deformation at fixed capillary number, Ca, decreased and the critical capillary number for droplet breakup increased. For a 20% dispersed phase blend, the steady-

state capillary number calculated from the volume-averaged droplet diameter increased with increasing droplet-phase elasticity, but was smaller than for isolated droplet. They suggested that increasing shear rate in concentrated blends was more important than coalescence in influencing steady-state droplet size.

Recently, viscoelastic mode of droplet deformation and droplet extension in the vorticity direction was reported by Cherdhirankorn et al.[11]. They investigated viscoelastic droplets in an immiscible viscoelastic matrix for blend of elastic polystyrene droplets dispersed in an elastic high density polyethylene matrix in a simple shearing flow between two transparent parallel disks by selecting two blends system with viscosity ratio near unity, but at different elastic ratios between the droplets and the matrix phases. They found that, in system A with higher elasticity, the droplets initially deformed in the flow direction after startup of steady shear but then began reverting to a spherical shape, and eventually deformed in the vorticity direction. In system B with lower elasticity, the droplet first deformed in the shear direction, and thereafter continuously contracted in the flow direction until it reached its steady-state shape. Moreover, the droplet deformed increasingly along the vorticity with increasing capillary number, and above a critical capillary number Ca_c, breakup occurred. Levitt and Macosko[12] studied the blends of polypropylene drops of various viscosity and elasticity ratios. Drops were sheared in a polystyrene matrix by using two transparent counter-rotating parallel disks which provided simple shear flow. They found that highly elastic drops forming the minor phase stretched perpendicular to the flow direction and the width of the flattened drops depended on the difference in elasticities between the matrix and the drop or the second normal stress differences of the two phases.

K.B. Migler[13] studied droplet vorticity alignment in model polymer blends by using polymethylsiloxane as the matrix phase and a polybuthylene as the droplet phase under a shear flow. The viscosity ratio was near unity but the elasticity ratio of the droplet to the matrix was greater than 100. They found that in the limit of weak shear and small droplet ($Ca < 5$), the droplet alignment was along the flow direction, whereas for strong shear and large droplets ($Ca > 5$), the alignment was along the vorticity direction where the distribution of aspect ratio was broad. Mighri and Huneault[14] studied the deformation and breakup mechanisms of viscoelastic drops

(Boger fluid) in a Newtonian matrix (PDMS) in a shearing flow in a transparent Couette flow cell. At low shear rate, the authors found that the dispersed drop was oriented along the flow field and drop deformation increased with shear rate, as expected. However, when a critical shear rate was reached [$Ca_c \approx 5.5$], the deformed drop began to contract in the flow direction. When increasing the shear rate over this critical value drop contraction occurred and was followed by elongation perpendicular to the flow direction. This elongation increased with shear rate until the final breakup occurred.

In this work, the behavior of immiscible blend morphology namely the transient and steady state droplet deformation and the breakup was investigated. The effect of the viscosity ratio 0.5, 1.0 and 2.6, and the effect of capillary number and elasticity were studied by using a flow cell mounted on an optical microscope where transient and steady state deformations of isolated droplets in simple shearing flow were observed.

II. EXPERIMENTS

A. Materials

The materials used in this study were two grades of high-density polyethylene (HDPE1 and HDPE2) as the matrices, donated by Bangkok Polyethylene and Aldrich (Catalog numbers are 1600J and 42,801-9, respectively). The molecular weight are 68,000 g/mol for HDPE1. The melt flow indices are 14 and 42 g/10min for HDPE1 and HDPE2 respectively. Two grades of polystyrene (PS1 and PS2) used as dispersed phases, were purchased from Polysciences (Catalog numbers are 23,637 and 18,544 respectively). Their molecular weights are 61,000 and 62,000 g/mol for PS1 and PS2, respectively Both grades of the polystyrene resins were crushed to small pieces and their sizes were controlled by passing the flakes though a 425 μm sieve. All polymers were heated at 80°C under vacuum for 12 hours to eliminate any volatile substances.

B. Rheological Characterization [Lerdwijitjarud][9] and [Cherdhirankorn][11]

Rheological properties of our materials had been previously measured in the previous work[Lerdwijitjarud][9] and [Cherdhirankorn][11], and the desired pairs of polymers and operating temperatures were selected for this study. The steady-state shear viscosity and the first normal stress difference of each polymer were measured by a cone-and-plate rheometer [Rheometric Scientific, model ARES] (25-mm plate diameter with cone angle 0.1 rad). The rheological properties were obtained at the shear rates ranging between 0.1 and 1 s^{-1} using the shear rate sweep test mode, and the transient test mode was used when the shear rate was higher than 1 s^{-1}.

C. Observation of an Isolated Droplet in Shearing Flow

1. Shearing Apparatus

To generate simple shear flow and to observe droplet behaviors, we used a flow cell device (Linkam CSS 450, Linkam Scientific Instruments Ltd., UK) with two quartz parallel disks attached to an optical microscope (Leica DMRPX, Leica Imaging Systems LTd., Cambridge, England). The images were recorded by a CCD camera (Cohu 4910, Cohu Inc., CA). They were analyzed on a computer using the Scion image software (http://wwwscioncorp.com).

2. Sample Preparation

HDPE was molded in the form of disks 25-mm diameter and 0.5-1 mm thick by compression molding at 140°C under the pressure of 10 tons for 1 minute. Drops of PS were injected into the matrix by means of a microsyring, and covered with another HDPE disk to form a sandwich. The sandwich was placed on the bottom disk of the flow cell, and then covered with the top disk of the flow cell. The sample was held at the testing temperature until complete letting occurred.

3. Determination of Relaxation Time

The sample was inserted between the two glass surfaces of the flow cell, whose roles were to maintain a constant specimen thickness and to ascertain that the imposed shear deformation was uniaxial. The sample was heated to the temperature chosen for the measurement. The desired strain was imposed onto a selected drop which moved the droplet out of the viewing window. The droplet then was allowed to completely relax into a spherical shape during a period of at least 60 min, and then the droplet was subjected to the same strain in the opposite direction in order to bring the droplet back into the viewing window. Observation of retraction of the ellipsoidal droplet was carried out by using an optical microscopic at a magnification depending

on the drop-size. Around 100 to 200 droplet images were recorded (10-20 second/frame). The deformation parameter, Def*, of a retracting droplet vs. time was measured; it is known to decay exponentially [Luicinia et al. (1997)][15] from the proposed equation.

$$Def^* = Def^*_0 \exp [-t/\tau] \quad (4)$$

The slope of Def* vs. t on a semi-log plot can be related to the characteristic relaxation time for a single drop, τ, and the interfacial tension calculated from the following relation:

$$\tau = \frac{(3 + 2\eta_r)(16 + 19\eta_r) r_o \eta_{m,o}}{40(1 + \eta_r)\Gamma} \quad (5)$$

To study the effect of droplet size on interfacial tension, the droplet size was varied from 70 μm to 400 μm at the fixed strain of 2 strain and the effect of strain on the interfacial tension was then studied by varying strain from 1-8% with the fixed size of droplet at 370 ± (10μm). The apparent interfacial tension values inferred from Eq. 5 increase with the droplet size. The apparent interfacial tension obtained for large droplet is expected to be the most accurate in which it does not depend on strain.

In principle, Eq. 5 is valid only for Newtonian systems, therefore interfacial tension for the polymerblend systems used in this work were taken from the literature [Brandrup and Immergut (1989)][16], which are 5.84 mN/m for system A at 143°C, 5.60 mN/m for system B at 155 °C, 5.92 mN/m for system C at 139 °C, and 5.76 mN/m for system D at 147 °C.

Since the images of the deformed droplet were captured only in the plane perpendicular to the shear gradient direction, the true length of the principal axes of the ellipsoidal droplet could not be determined directly. The lengths of principle axes can be determined by using the orientation angle (θ), which is the angle of the major axis of the deformed droplet in the flow-flow gradient plane

Even if the lengths of the principal axes can be determined by using the method mentioned above, the lengths of the observable axes were used here to describe the behavior of each droplet by defining a modified deformation parameter Def* as:

$$\mathbf{Def^* = (a^*-c)/(a^* +c)} \qquad (6)$$

where the asterisk denotes that the deformation parameter is an apparent one obtained from the droplet image projected into the flow-vorticity plane; see Fig 4.1.

4. Transient Deformation

The matrix phase was loaded into the flow cell and various single droplets were subsequently immersed into the matrix. The deformed shapes of the droplets were observed as a function of time from the initial instant to it attained steady-state shapes. Because of the limitation of flow cell device, a single droplet can not be imaged from the startup of shearing until attaining steady-state shape. Therefore the deformed shapes of isolated droplet could be determined by combining the results of several experiments. In the experiment of type 1, the droplet moved out of viewing window through imposing low strain of less than 40 strain units (≈ 1 orbit) on the droplet. The droplet was left to relax its shape at least 60 minutes. Then the isolated droplet was imposed by the same strain but in the opposite direction which moved the droplet back into the viewing window, where we could image its deformation. However, the droplet could not be observed for large strain as it would move out of the viewing window. To obtain deformation of droplet at large strains, in the experiment of type 2, the droplet was imposed with a shearing flow continuously and images of the droplet were taken when the droplet passed through the viewing window. To clearly obtain droplet images, we stopped the flow each time the droplet reached the viewing window for a period of less than 1 second; this duration was relatively short for droplet to relax its shape by a significant amount. The time for one cycle of a droplet was recorded with a stopwatch along with the time shown on the Linksys program, and then the flow was imposed again until the droplet passed through the viewing window again. By repeating the experiment on droplets which were stopped at different times, we could assemble a consistent curve of deformation

from the initial time to the time in which droplets attained steady-state shape. Transient experiments were achieved by varying the capillary number, Ca, from 5, 8, to 11 through varying droplet size at the same shear rate of 0.4 s^{-1}. To separate the effect of viscous force from the effect of elasticity, other experiments were carried out by keeping capillary number fixed at 8 and the elastic forces were varied by changing the shear rate from 0.10, 0.17, 0.40 to 0.63 s^{-1} and while using the droplet sizes of 289.7, 177, 85 and 56 μm, respectively. Transient experiments for system B were carried out by keeping capillary number at 8 at the shear rate of 0.63 s^{-1}.

5. Steady-State Deformation and Breakup

The sample was loaded into the flow cell, droplet was left to relax to form spherical shapes for a period of at least 70 min; this was a little longer than the duration of the transient experiment because some droplets used here were larger. The steady-state shearing mode was used, steady-state shapes of isolated droplets below the critical capillary number for droplet breakup were determined. The critical capillary number was determined by imposing successive changes of initial droplet size from small droplet size to larger droplet size at a fixed shearing rate at 0.4 s^{-1} for system A and system C and a fixed shearing rate at 0.63 s^{-1} for system B until the drop breakup was observed. To determine the steady-state droplet shape as a function of capillary number, the required strain to reach steady-state droplet shape depended on droplet size which increased with the droplet size. From the transient experiment, the required strain to reach steady-state droplet shape was determined and found to be around 4000 strain, at Ca = 8 and D_0 = 85 (± 5μm) . Therefore a constant shear rate was then applied until a strain exceeding 4,000 strain units was attained. To ensure that the steady-state deformation had been attained, when a selected droplet passed through the viewing window, the droplet was imaged over a period of 5 to 10 min and we measured Def* until its value became constant. After that, flow was stopped and the droplet shape relaxation was recorded with the CCD camera at speeds of 10-20 second per frame for approximately 90 minutes.

For droplets in which no steady-state shape was obtained, the unstable shapes of the droplets were recorded with time until the droplets were broken. The breakup processes for system A were achieved by keeping capillary number fixed at 11 using shear rates of 0.40 s^{-1}; for system B capillary number was fixed at 9.5 and shear rates were 0.20, 0.63 s^{-1}.

III. RESULTS AND DISCUSSION

A. Transient Deformation in Steady Shear Flow

1 Effect of Ca on Droplet Deformation

The effect of capillary number, Ca, on the droplet transient deformation, during a small strain period (less than 40) and during a large strain period (greater than 40) for the system A was investigated. The conditions of the experiment are: a fixed shear rate of 0.4 s^{-1}, a fixed Weisenberg number, Wi_d of 0.75, a fixed viscosity ratio of 2.6, and the capillary number, Ca was varied from 5, 8, and 11 by varying the droplet size to be at 52 (±5), 85 (±5), 125 (±7) μm, respectively. The parameters of this experiment are tabulated in Table 2.

Figure 2a displays the transient deformation, Def*, vs. strain between 40 and 4000 at three Capillary numbers: 5,8, and 11. During this strain period, Def* first becomes negative and reaches a minimum at strain around 300. At strains larger than 300, Def* increases toward zero, the state of no deformation, at strain around 900 before decreases toward its equilibrium Def* values of -0.065 and -0.205, for Ca equal to 5 and 8, respectively. For Ca equal to 11, there is no steady state value of Def*; all drops eventually break apart. Figures 2b and 2c show the corresponding evolutions of a^*/D_o and c/D_o vs. strain between 40 and 4000. a^*/D_o decreases towards a minimum at strain equal to 300, rises to a maximum at 900, and then decreases towards its steady state Def* values of 0.956 and 0.882, for Ca equal to 5 and 8, respectively. For Ca equal to 11, a* continues to decrease beyond strain of 900 until strain of 4000, where breakup occurs. c/D_o, however, monotonically increases

with increasing strain between 40 and 4000; its steady state values are (1.088) and (1.336) for Ca equal to 5, and 8, respectively. At Ca equal to 11, c/D_o and the strain values at breakup are equal to 5.180 and 4073, respectively. At this Weisenberg number, Wi_d equal to 0.75 and the viscosity ratio of 2.6, drops eventually elongate in the vorticity direction, and shrink in the flow direction; the critical Capillary number is approximately equal to 11.

Figures 2d-2f show the evolutions of Def*, a^*/D_o, and c/D_o vs. strain between 0 and 40, the initial period. All three deformation parameters oscillate three cycles with differing amplitudes during this period. The amplitude of oscillation increases with the Capillary number Ca. The initial oscillations and the magnitudes of the oscillation (η_r=2.6, Wi_d = 0.75, Ca = 5, 8, 11) seen here are in agreement with those found previously[11](η_r=1.0 should this be , Wi_d = 0.30, Ca =8).

2. Effect of Elasticity on Droplet Deformation

Next we investigate the influence of the droplet elasticity on the droplet transient deformation. The system investigated is the system A where the viscosity ratio is 2.6, the Capillary number Ca is fixed at around 8.0, and the shear rate is varied from 0.17, 0.40 to 0.63 s^{-1}corresponding to the Weisenberg numbers of 0.45, 0.75 and 0.99, respectively. In order to keep Ca number fixed at 8.0, the droplet sizes subject to these shear rates are chosen to be 177.3, 86.8, and 56 (±2), respectively. Figures 3a-3c show the evolutions of Def*. a^*/D_o, and c/D_o vs. strain between zero and 6000. Def* first decreases to a negative minimum at strain 300, rises towards a positive maximum at strain around 900, and then decreases towards its steady state values at strain above 3000. The negative minimum Def* values are -0.100, -0.107, and -0.114. The positive maximum Def* are 0.109, 0.032 and 0.019. The corresponding steady state negative Def* values are -0.230, -0.205 and -0.142, respectively. Therefore, it appears the amplitudes of the negative minimum and the steady state Def* increase with increasing droplet elasticity, whereas the amplitude of the positive maximum Def* decreases with increasing droplet elasticity. The initial decrease of Def* towards its negative minimum, for strain between 0 to 300, is

largely due to the initial stretching of droplets along the vorticity direction (Fig. 3c), whereas the rise towards positive Def* maximum at strain 900 is due to the droplet stretching along the flow direction (Fig 3b). We may note that by varying the shear rate we were able to vary both Wi_d and Wi_m the ratio between elastic force and the shear force, where Ca and $N_{1,r}$ are fixed at 8 and at around 3, respectively (Table 2).

3. Effect of Viscosity Ratio on Droplet Deformation

For the effect of viscosity ratio on the droplet transient deformation, experiments were carried out with the Capillary number, Ca, fixed at 8.0 and the Weisenberg number, Wi_d fixed at 0.30. Systems investigated are systems A, B and D whose experimental conditions and rheological properties are tabulated in Table 3. Figure 4a compares the evolutions of Def* of systems A, B, and D whose viscosity ratios are 2.6, 0.5 and 1.0, respectively. Def* initially decreases from zero towards its minimum of about -0.12 at strain around 300, then rises to a positive maximum at strain depending on the viscosity ratio. For viscosity ratios equal to 2.6 and 1.0 (systems A and D), the maximum Def* occurs at strains around 1500 and 900 with corresponding amplitudes of 1.4 and 0.8, respectively. For the viscosity ratio equal to 0.5 (system B), the maximum Def * occurs at a lower strain of about 500 and with a higher amplitude of about 0.16. On the other hand, the steady state Def* values are -0.22, -0.12, -0.12 for the systems with the viscosity ratios of 2.6, 1.0 and 0.5, respectively. Figures 4b and 4c show the corresponding evolutions of $a^*/D_o$and c/D_o. The initial decrease in Def* towards its negative minimum can be attributed to the steep rise in c/D_o or the initial droplet stretching along vorticity direction. The subsequent increase in Def* towards its positive then can be attributed to the increase in a^*/D_o or the stretching along flow direction. We may note that, from Table 3, Wi_d of the three systems are nearly the same: about 0.3 In summary, the effect of viscosity ratio is to change the oscillation amplitude, the oscillation period, and the steady state values of Def*.

Figures 5a and 5b show two sequences of transient deformation of systems A and B, having the same Wi_d of 0.30 and Ca =8.0. The difference between

the two systems is the viscosity ratios: 2.6 vs. 0.5, respectively. Here we see that both droplets finally attain the steady state shapes with negative Def^*_{ss}; the former system stretches more along the vorticity direction.

B. Steady-State Deformation

The steady state deformation refers to the final shape of droplets after transient behaviors have ceased. Figure 6a shows Def* vs. Ca of systems A, B, and C and D corresponding to the viscosity ratios of 2.6, 0.5, 1.0, and 1.0, respectively. In these systems, the droplet Weisenberg numbers, Wi_d are fixed 0.34, 0.28, 0.005, and 0.3 respectively. The capillary number was varied by choosing drops of various sizes. To obtain and to determine the steady-state droplet shape as a function of capillary number, a sufficient strain to reach a steady state was required. On comparing data of systems, A, B, and D, it is evident that negative Def^*_{ss} value at a given Ca decreases with increasing viscosity ratio, η_r, and the droplet Weissenber number, Wi_d. On the other hand, for systems C and D both having viscosity ratio equal to 1, we find that negative Def^*_{ss} value decreases with increasing Wi_d. Therefore, droplet elasticity appears to be the dominating factor for droplets to stretch along the vorticity direction. It is interesting to note the steady state data of system C; Def^*_{ss} values are quite close to zero and vary slightly with increasing Ca between 2-8. Thus, it is possible to chose a system at very low Wi_d (0.005) such that droplets do not deform as Ca is increased. Figures 6a and 6b show the corresponding evolutions of a^*/D_o and c/D_o. Due to scatters of data, we can only infer that the function a^*/D_o vs.Ca depends weakly on viscosity ratio and the droplet Weissenberg number. On the other hand, steady state c/D_o increases with viscosity ratio for comparable Wi_d (Systems A and B), and increases with Wi_d for the same viscosity ratio (systems C and D).

C. The Critical Capillary Number

The critical Capillary number for drop breakup to occur was determined for systems A, B, and D, corresponding to the viscosity ratios of 2.6, 0.5, and 1.0, respectively. The corresponding fixed Wi_d values are 0.34, 0.28, and 0.30, respectively. In each system, the shear rate was fixed and drops of various sizes were chosen in order to vary the Capillary number.

The critical capillary numbers, Ca_c, are 9.44, 8.95, and 9.10 for system A, B, and D[11] respectively. Corresponding droplet sizes investigated are 115.0, 79.0, and 92 μm whose critical Def^*_c are around –0.32, -0.18, and -0.27. Thus, for comparable Wi_d, Ca_c increases with viscosity ratio. We were not able to observe the breakup condition of system C, presumably because the steady state deformation of this system is very small.

D. Droplet Breakup Mechanism

Here, we investigate the droplet breakup sequences of systems A and B. The shear rate used for system A is 0.40 s^{-1} at Ca = 11 (slightly beyond Ca_c) and Wi_d = 0.71. For system B, the shear rate used is 0.63 s^{-1} at Ca = 9.5 (slightly beyond Ca_c). We can see that in both systems, η_r = 2.6 and 0.5, and at these conditions droplets follow the oscillation patterns as described previously, and eventually breakup in the vorcitiy direction, with an S shape as the final droplet shape. A minor difference between the breakup patterns of systems A and B is that for system B whose viscosity ratio is smaller (0.5), there is a more pronounced stretching along the flow direction. Another breakup sequence for system B is shown in Fig. 9. The shear rate used is lower, i.e. 0.20 s^{-1}, and therefore Wi_d is 0.25 which lower than that of Fig.8, but the viscosity ratio and the Capillary number remain at 0.5 and 9.5, respectively. Here, we can see that at a lower Wi_d the drop breakups mainly along the flow direction. The final shape prior to the breakup, the droplet assumes a dumbell shape.

Therefore, the breakup along the vorticity direction is a consequence of elasticity, presumably of the droplet and the matrix.

IV. CONCLUSIONS

We observed the transient deformation, under a startup of a steady shear flow, of droplets in the systems whose viscosity ratios are 0.5, 1.0 and 2.6. Droplet Def* generally oscillates for three cycles, with the amplitudes and the periods of oscillation depending on the Capillary number,Ca, the Weissenberg number, W_{id} and the viscosity ratio. Larger amplitudes and larger osciilations periods are found for strains between 40-6000. The negative steady state Def* value decreases with Ca and Wi_d presumably due to the effects of droplet and matrix elasticity. Surprisingly, we were able to select a system under appropriate conditions such that droplets do not deform within the range of Ca between 2 and 8. Droplets breakup in the vorticity direction if Wi_d is suuficiently high. We also find that for a lower Wi_d, the breakup can occur in both the vorticity and the flow direction. When Wi_d is sufficiently low, the breakup occurs only along the flow direction.

ACKNOWLEDGEMENTS

The author, A.S., would like to acknowledge the supports from the Postgraduate Education and Research Programs in Petroleum and Petrochrmical Technology (PTT Consortium), the Conductive and Electroactive Polymers Research Unit (CU-Rachadapisek), and the financial support from Thailand Researh Fund, grant no. BRG4680015.

F 7161193

REFERENCES

[1]G. I. Taylor, "The viscosity of a fluid containing small drops of another fluid," Proc. R. Soc. London, Ser. A **138**, 41 (1932).

[2]G. I. Taylor, "The formation of emulsions in definable fields of flow," Proc. R. Soc. London, Ser. A **146**, 501 (1934).

[3]T. Tsakalos, N. Patrick, and P. D. Edith, "Deformation and breakup mechanisms of single drops during shear," J. Rheol. **42**, 1403 (1998).

[4]J. W. Ha and L. G. Leal, "An experimental study of drop deformation and breakup in extensional flow at high capillary number," Phys. Fluids **13**, 1568 (2001).

[5]H. P. Grace, "Dispersion phenomena in high viscosity immiscible fluid systems and application of static mixers as dispersion devices in such systems," Chem. Eng. Commun. **14**, 225 (1982).

[6]T. Tavgac, Ph.D. thesis (Chemical engineering), Univ. of Houston, Houston, Texas, (1972).

[7]F. Mighri, A. Ajji, and P. J. Carreau, "Influence of elastic properties on drop deformation in elongational flow," J Rheol **41**, 1183 (1997).

[8]F. Mighri, P. J. Carreau, and A. Ajji, "Influence of elastic properties on drop deformation and in shear flow," J Rheol **42**,1477 (1998).

[9]W. Lerdwijitjarud, A. Sirivat, and R. G. Larson, "Influence of elasticity on dispersed-phase droplet size in immiscible polymer blends in simple shearing flow," Polym. Eng. Sci. **42**, 798 (2002).

[10]W. Lerdwijitjarud, R. G. Larson, and A Sirivat, "Influence of weak elasticity of dispersed phase on droplet behavior in sheared polybutadiene/ Poly(dimethylsiloxane) blends," J Rheol. **47**, 37 (2003).

[11]T. Cherdhirankorn, "Dynamics of vorticity stretching and breakup of isolated viscoelastic droplet in an immiscible viscoelastic matrix," Rheol Acta 43, 246 (2004).

[12]L. Levitt, C. W. Macosko, and S. D. Pearson, "Influence of normal stress difference on polymer drop deformation," Polym. Eng. Sci. **36**, 1647 (1996).

[13]K. B. Migler, "Droplet vorticity alignment in model polymer blends," J. Rheol. **44**, 277 (1999).

[14]F. Mighri, and M. A. Huneault, "Dispersion visualization of model fluids in a transparent Couette flow cell," J. Rheol. **45**, 783 (2001).

[15]A. Luciani, M. F. Champagne, and L. A. Uttacki, "Interfacial tension coefficient from the retraction of ellipsoidal drops," Polym. Phys. **35**, 1393 (1997).

[16]J. Branrup, and E. H. Imergut, Polymer Handbook, 3rd Ed., New York (1989).

TABLES

Table 1 Polymer blend systems

Blend system	Blend components (Drop/Matrix)	Temperature (°C)	Viscosity ratio (η_d/η_m)
A	PS1/HDPE1	143	2.6
B	PS2/HDPE1	155	0.5
C	PS1/HDPE2	139	1.0
D	PS2/HDPE1	147	1.0

D is the system A of Cherdhirankorn *et al.*[11]

Table 2 Data of Figures 2 and 3: system A (PS1/HDPE1) at shear rate of 0.4 s^{-1} Wi_d = 0.75, Ca is varied (5,8,11) corresponding to the initial droplet sizes ≈ 52, 85, 125 μm; and the blend system A (PS1/HDPE1), Wi_d is varied (0.45,0.75,0.99)

Shear rate (s^{-1}) / Data	0.17	0.40	0.63
Temperature (°C)	143	143	143
η_d: Viscosity of the droplet phase (Pa.s)	7,616	6,880	6,340
η_m: Viscosity of the matrix phase (Pa.s)	2,872	2,580	2,440
η_r: Viscosity ratio	2.6	2.6	2.6
Γ: Interfacial tension (mN/m)	5.84	5.84	5.84
$N_{1,d}$: First normal stress difference of the droplet phase (Pa)	620	2,080	3,950
$N_{1,m}$: First normal stress difference of the matrix phase (Pa)	208	733	1,230
$N_{1,r}$: First normal stress difference ratio	2.97	2.83	3.20
Ca : Capillary number	8	5, 8, 11	8
D_0 : Initial droplet size (μm)	177	52, 85, 125	56
Wi_d: Weissenberg number of the dispersed phase	0.45	0.75	0.99
Wi_m: Weissenberg number of the matrix phase	0.43	0.71	0.80

$$Ca = \frac{D_0 \dot{\gamma} \eta_m}{2\Gamma}$$

$$Wi_d = N_{1,d}/(\eta_d \dot{\gamma})$$

$$Wi_m = N_{1,m}/(\eta_m \dot{\gamma})$$

Table 3 Blend systems investigated in Figure 4

Blend system(drop/matrix)	System A (PS1/HDPE1)	System B (PS2/HDPE1)	System D (PS2/HDPE1)
Data			
Temperature (°C)	143	155	147
Shear rate (s^{-1})	0.10	0.63	0.50
η_d: Viscosity of the droplet phase (Pa.s)	7,996	964	2,323
η_m: Viscosity of the matrix phase (Pa.s)	3,026	2,013	2,331
η_r: Viscosity ratio	2.6	0.5	1.0
Γ: Interfacial tension (mN/m)	5.84	5.60	5.79
$N_{1,d}$: First normal stress difference of the droplet phase (Pa)	276	168	-
$N_{1,m}$: First normal stress difference of the matrix phase (Pa)	78.3	920	834
$N_{1,r}$: First normal stress difference ratio	3.52	0.18	-
G'_d: Storage modulus of the droplet phase (Pa)	-	-	179
G'_m: Storage modulus of the matrix phase (Pa)	-	-	248
G'_r: Storage modulus ratio	-	-	0.72
Wi_d: Weissenberg number of the dispersed phase	0.34	0.28	0.30
Wi_m: Weissenberg number of the matrix phase	0.26	0.72	0.71

Table 4 Blend systems investigated in Figure 5

Blend system(drop/matrix) Data	System A (PS1/HDPE1)	System B (PS2/HDPE1)	System C (PS1/HDPE2)	System D (PS2/HDPE1)
Temperature (°C)	143	155	139	147
Shear rate (s^{-1})	0.10	0.63	0.40	0.50
η_d: Viscosity of the droplet phase (Pa.s)	7,996	964	630	2,323
η_m: Viscosity of the matrix phase (Pa.s)	3,026	2,013	595	2,331
η_r: Viscosity ratio	2.6	0.5	1.0	1.0
Γ: Interfacial tension (mN/m)	5.84	5.60	5.92	5.79
$N_{1,d}$: First normal stress difference of the droplet phase (Pa)	276	168	-	-
$N_{1,m}$: First normal stress difference of the matrix phase (Pa)	78.3	920	-	834
$N_{1,r}$: First normal stress difference ratio	3.52	0.18	-	-
G'_d: Storage modulus of the droplet phase (Pa)	-	-	≈1.3	179
G'_m: Storage modulus of the matrix phase (Pa)	-	-	≈1.3	248
G'_r: Storage modulus ratio	-	-	1.0	0.72
Wi_d: Weissenberg number of the dispersed phase	0.34	0.28	≈0.005	0.30
Wi_m: Weissenberg number of the matrix phase	0.26	0.72	≈0.005	0.71

FIGURE CAPTIONS

Figure 1 Schematic drawing of a single drop observed from the side and top views of the optical microscope; a and b are the long and short axes of the droplet in the flow-gradient plane, a* is the a axis projected into the flow direction, and c is the principal axis in the radial direction.

Figure 2 Strain–dependent droplet deformation at various values of Ca for system A , controlled by changing the droplet diameter: [Ca = 5; Initial droplet size(μm): 52.3(■), 51.4(⊡), 51.7(▣), 52.0(◘), 50.5(◘),51.0(▩), 51.5(▣), 55.2(▣), 54.6(□);Ca = 8; initial droplet sizes(μm): 81.2(●), 80.8(⊙), 81.3(⊙), 87.5(⊙), 82.5(⊙), 80.2(⊙), 81.1(⊙), 85.3(⊙), 85.8(○); Ca = 11; initial droplet sizes(μm): 125.2( ), 120.3( ), 129.3( ), 119.1(▼), 127.6(▽)] at the same shear rate 0.4 s^{-1} , Wi_d = 0.75 (same elasticity) (a) Def* vs. strain, (b) a^*/D_0 vs. strain, (c) c/D_0 vs. strain. The strain–dependent droplet deformation during strain less than 40 : Ca = 5 droplet diameters are 50.5-55.2 μm (□); for Ca =8, droplet diameters are 80.2-87.5 μm (●); and Ca = 11, droplet diameters are119.1-129.3 (▽). (d) Def* vs. strain less than 40, (e) a^*/D_0 vs. strain less than 40, (f) c/D_0 vs. strain less than 40

Figure 3 Strain – dependent droplet deformation at different shear rates (different elasticities),. Ca = 8 is held fixed by varying the initial droplet diameter inversely with the shear rate for η_r = 2.6: (a) Def^* vs. strain, (b) a^*/D_0 vs. strain, (c) c/D_0 vs. strain. Three different shear rates were used (1): $\dot{\gamma}$ = 0.63 s^{-1}, Wi_d = 0.99 with D_0 = 57.7 μm (●) and repeat run at this shear rate with droplet size, 56.2 μm(○);(2): $\dot{\gamma}$ = 0.4 s^{-1}, Wi_d = 0.75 with D_0 = 86.8 μm(▲); (3): $\dot{\gamma}$ = 0.17 s^{-1}, Wi_d = 0.45, D_0 = 177.3 μm(□).

Figure 4 Dependence droplet deformation on applied strain at various viscosity ratios, η_r : Ca =8 and $Wi_d \approx 0.30$; η_r = 0.5, $\dot{\gamma}$ = 0.63 s^{-1}, (○); η_r = 1.0, $\dot{\gamma}$ = 0.50 s^{-1},

(●); $\eta_r = 2.6$, $\dot{\gamma} = 0.40\ s^{-1}$, (△). (a) Def* vs. strain, (b) a^*/D_0 vs. strain, (c) c/D_0 vs. strain.

Figure 5 Sequence of images of deformed droplets after startup of a steady shear $Wi_d \approx 0.30$, Ca = 8: (a) system A, $\eta_r = 2.6$ at a rate of 0.1 s^{-1}, $D_0 = 85.8$ μm ; (b) system B, $\eta_r = 0.5$ at a rate of 0.63 s^{-1}, $D_0 = 72.2$ μm.

Figure 6 Steady-state deformation: (a) steady-state deformation vs. Ca; (b) a^*/D_0 vs. Ca; and (c) c/D_0 vs. Ca. $Wi_d \approx 0.30$: system A with $\eta_r = 2.6$ at shear rate of 0.1 s^{-1}, (△); system D of Cherdhirankorn et al. (2004)[11] with $\eta_r = 1.0$ at shear rate of 0.5 s^{-1}, (○); system Bwith $\eta_r = 0.5$ at shear rate of 0.63 s^{-1}, (□); system C, $Wi_d \approx 0.005$, with $\eta_r = 1.0$ at shear rate of 0.4 s^{-1}, (▽), Ca is varied by varying droplet size.

Figure 7 Sequence of images of droplet breakup of system A at a shear rate of 0.40 s^{-1}, $D_0 = 125$ (±7) μm, $Wi_d = 0.75$ for $\eta_r = 2.6$, Ca = 11.

Figure 8 Sequence of images of droplet breakup of system B at a shear rate of 0.63 s^{-1}, $D_0 = 81.6$ μm, $Wi_d = 0.28$ for $\eta_r = 0.5$, Ca = 9.5.

Figure 9 Sequence of images of droplet breakup of system B at a shear rate of 0.20 s^{-1}, $D_0 = 225.3$ μm, $Wi_d = 0.25$ for $\eta_r = 0.5$, Ca = 9.5.

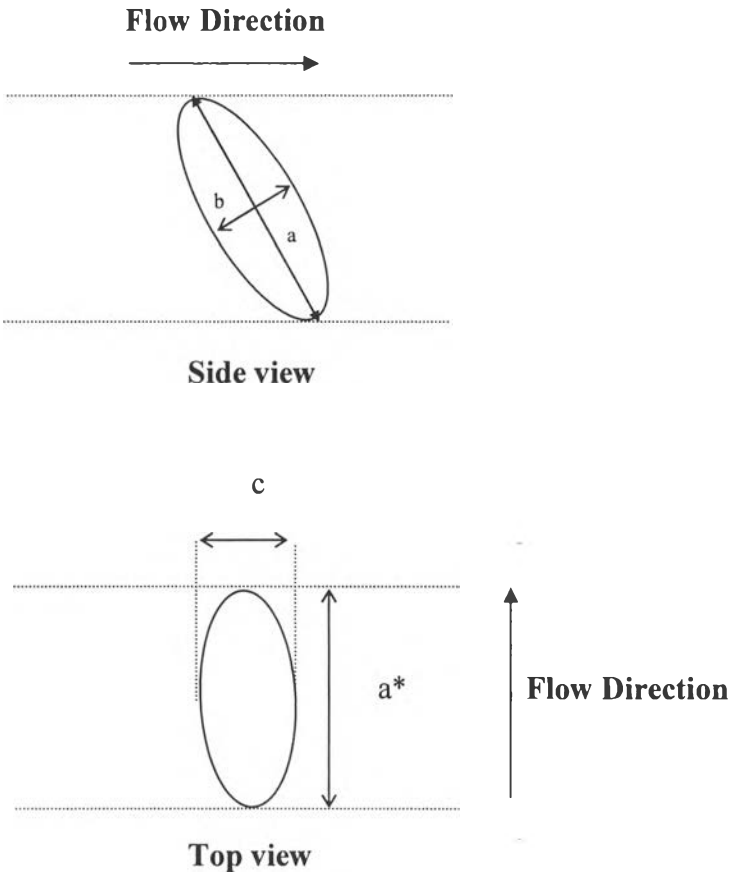

Figure 1 Schematic drawing of a single drop observed from the side and top views of the optical microscope; a and b are the long and short axes of the droplet in the flow-gradient plane, a* is the a axis projected into the flow direction, and c is the principal axis in the radial direction.

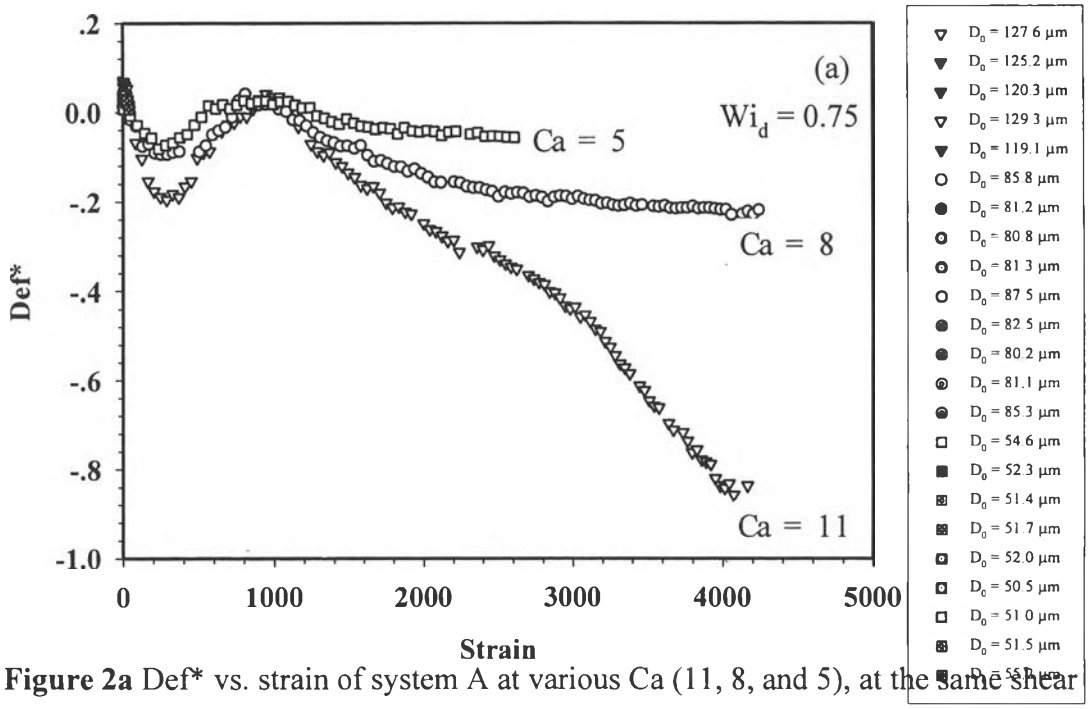

Figure 2a Def* vs. strain of system A at various Ca (11, 8, and 5), at the same shear rate of 0.4 s^{-1}, and $Wi_d = 0.75$.

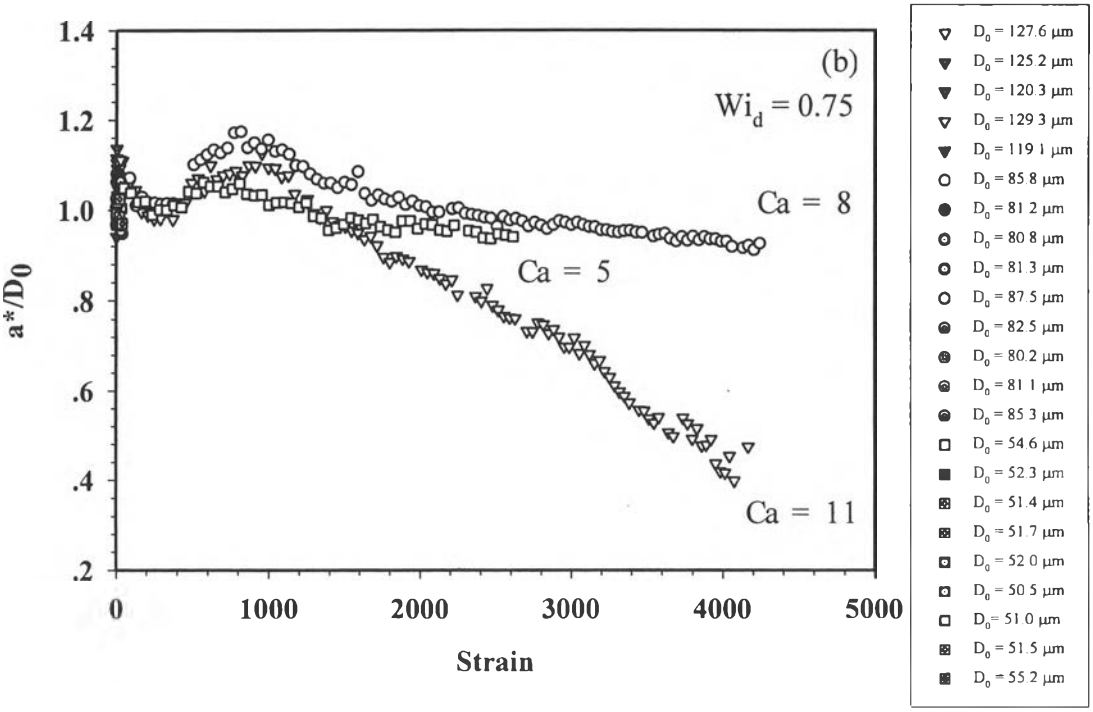

Figure 2b a^*/D_0 vs. strain of system A at various Ca (11, 8, and 5) at the same shear rate of 0.4 s^{-1}, and $Wi_d = 0.75$.

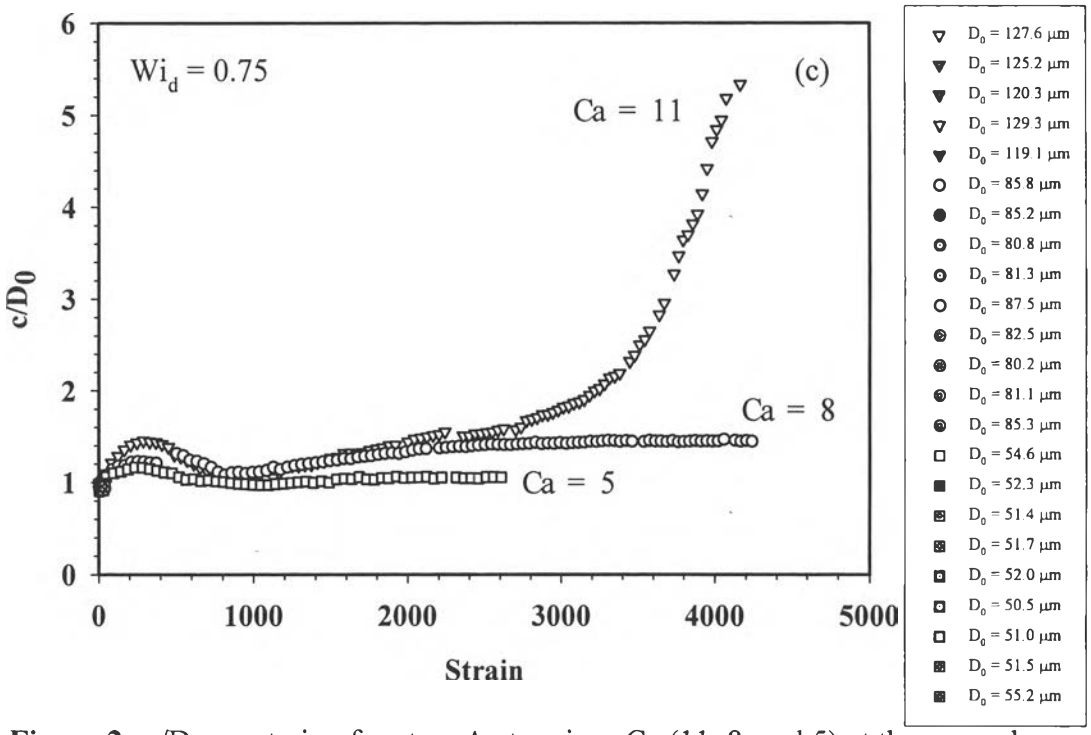

Figure 2c c/D_0 vs. strain of system A at various Ca (11, 8, and 5) at the same shear rate of 0.4 s^{-1}, and Wi_d = 0.75.

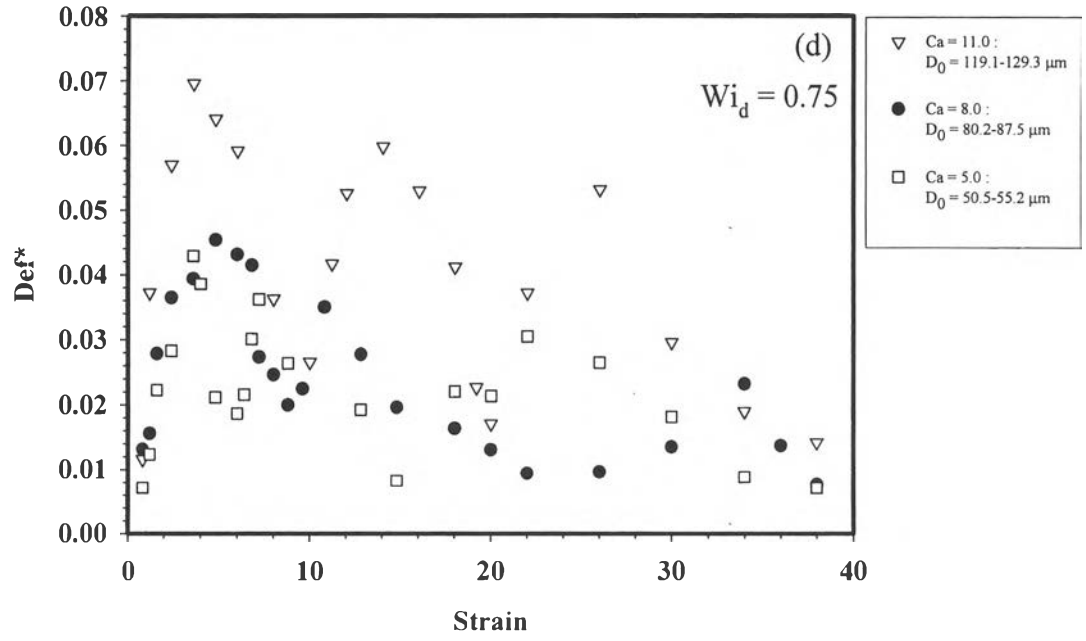

Figure 2d Def* vs. strain of less than 40 of system A at various Ca (11, 8, and 5) at the same shear rate of 0.4 s^{-1}, and Wi_d = 0.75.

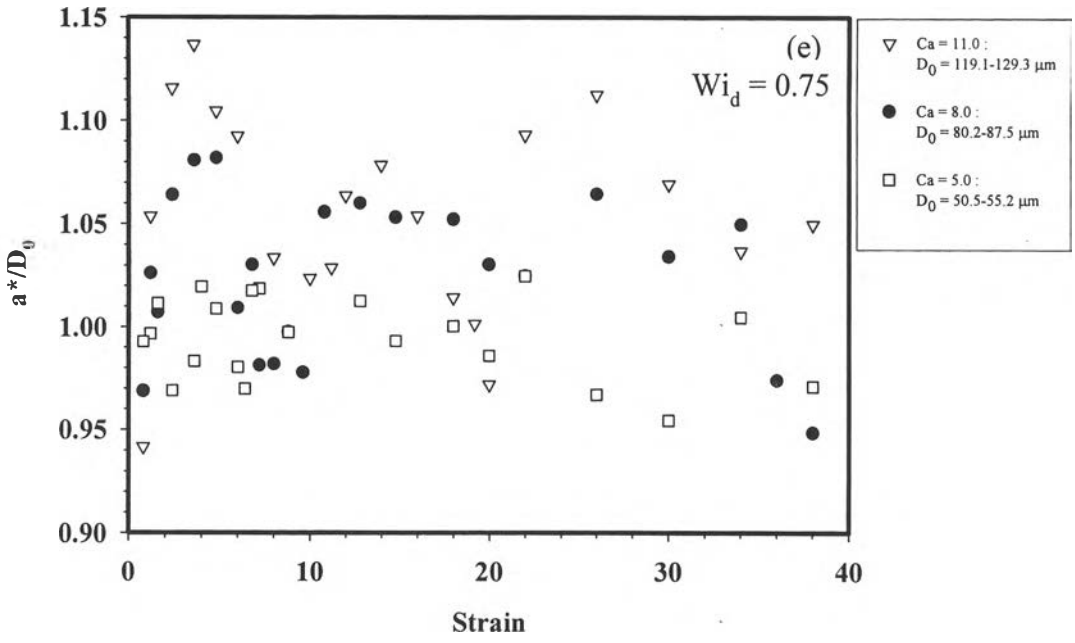

Figure 2e a^*/D_0 vs. strain of less than 40 of system A at various Ca (11, 8, and 5) at the same shear rate of 0.4 s^{-1}, and $Wi_d = 0.75$.

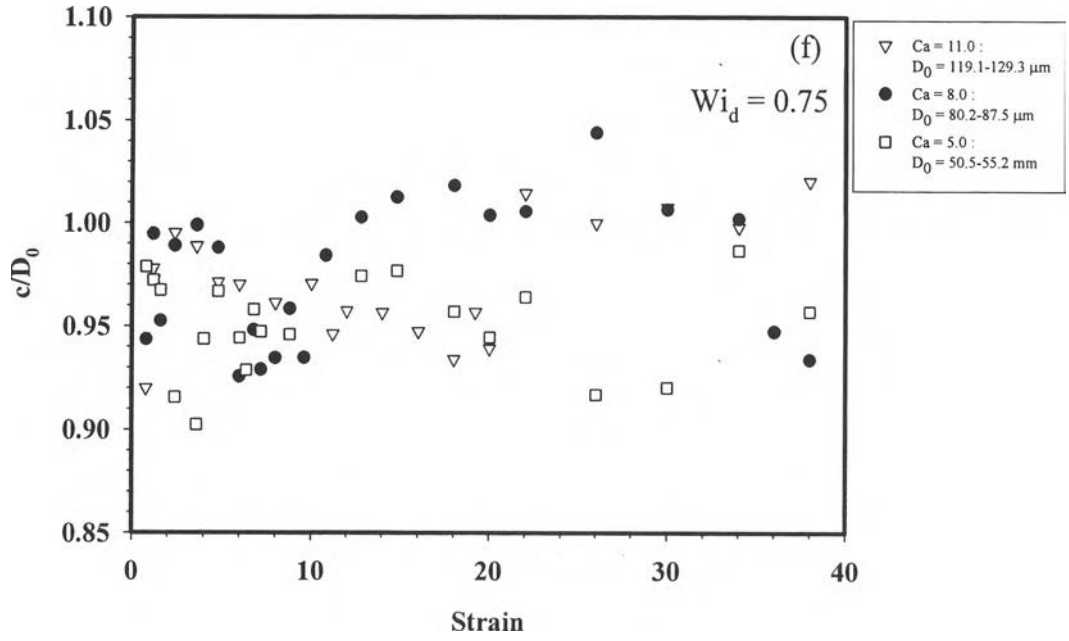

Figure 2f c/D_0 vs. strain of less than 40 of system A at various Ca (11, 8, and 5) at the same shear rate of 0.4 s^{-1}, and $Wi_d = 0.75$.

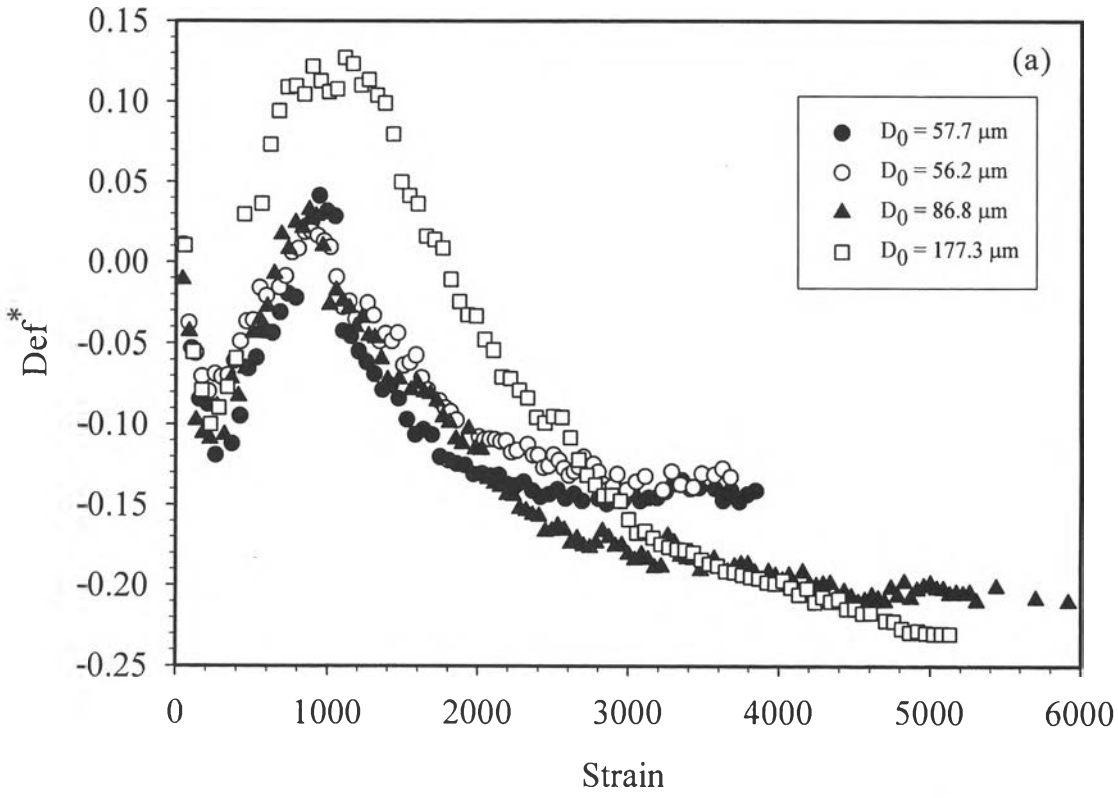

Figure 3a Def* vs. strain of system A at different shear rates, Ca = 8: $\dot{\gamma}$ = 0.17 s^{-1}, Wi_d = 0.45, (□); $\dot{\gamma}$ = 0.40 s^{-1}, Wi_d = 0.75, (▲); $\dot{\gamma}$ = 0.63 s^{-1}, Wi_d = 0.99, (●), (○).

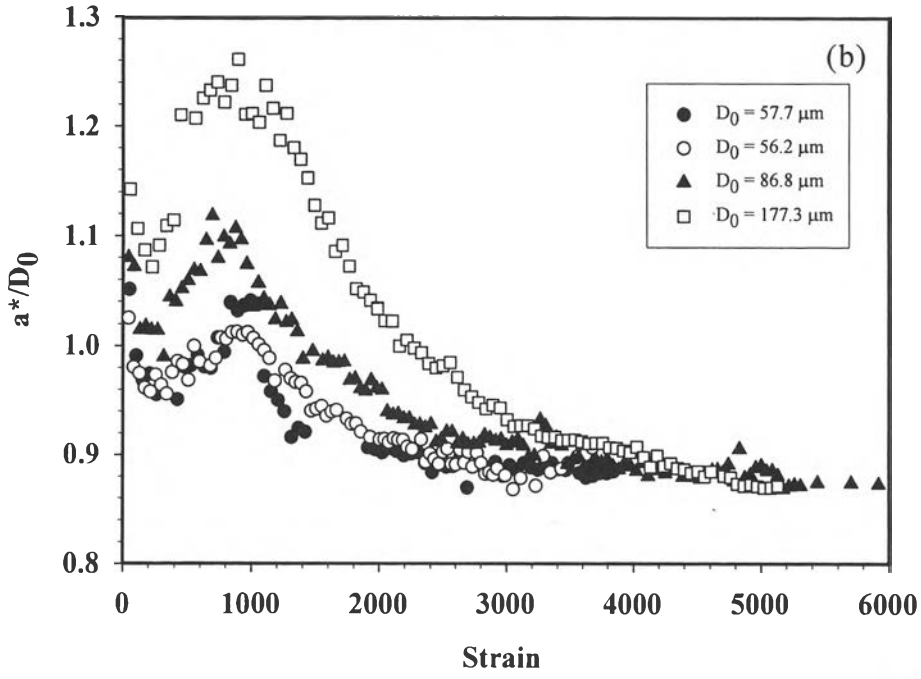

Figure 3b a^*/D_0 vs. strain of system A at different shear rates, Ca = 8: $\dot{\gamma}$ = 0.17 s^{-1}, Wi_d = 0.45, (□); $\dot{\gamma}$ = 0.40 s^{-1}, Wi_d = 0.75, (▲); $\dot{\gamma}$ = 0.63 s^{-1}, Wi_d = 0.99, (●), (○).

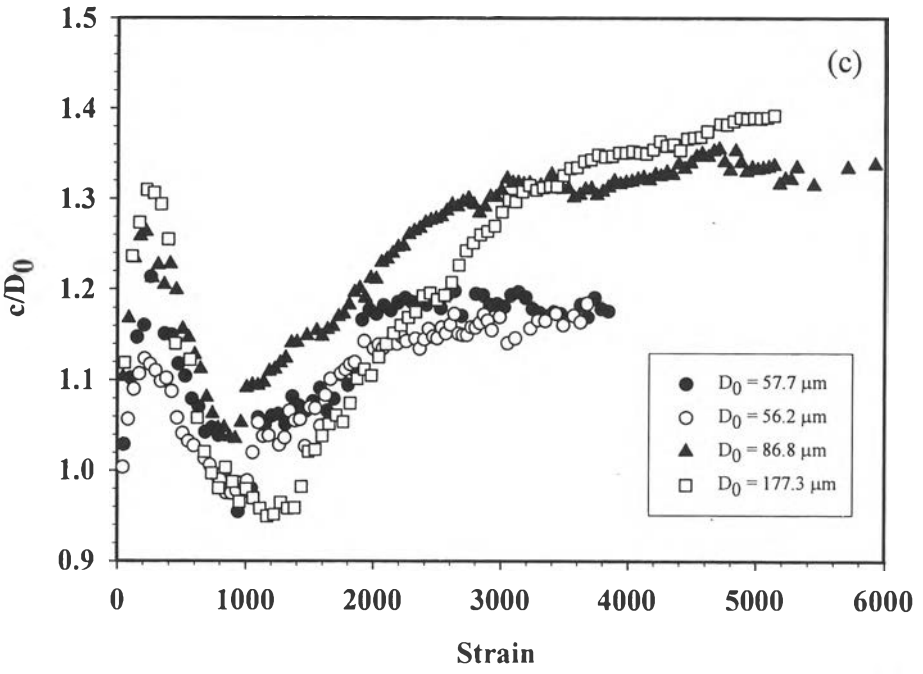

Figure 3c c/D_0 vs. strain of system A at different shear rates, Ca = 8: $\dot{\gamma}$ = 0.17 s^{-1}, Wi_d = 0.45, (□); $\dot{\gamma}$ = 0.40 s^{-1}, Wi_d = 0.75, (▲); $\dot{\gamma}$ = 0.63 s^{-1}, Wi_d = 0.99, (●), (○).

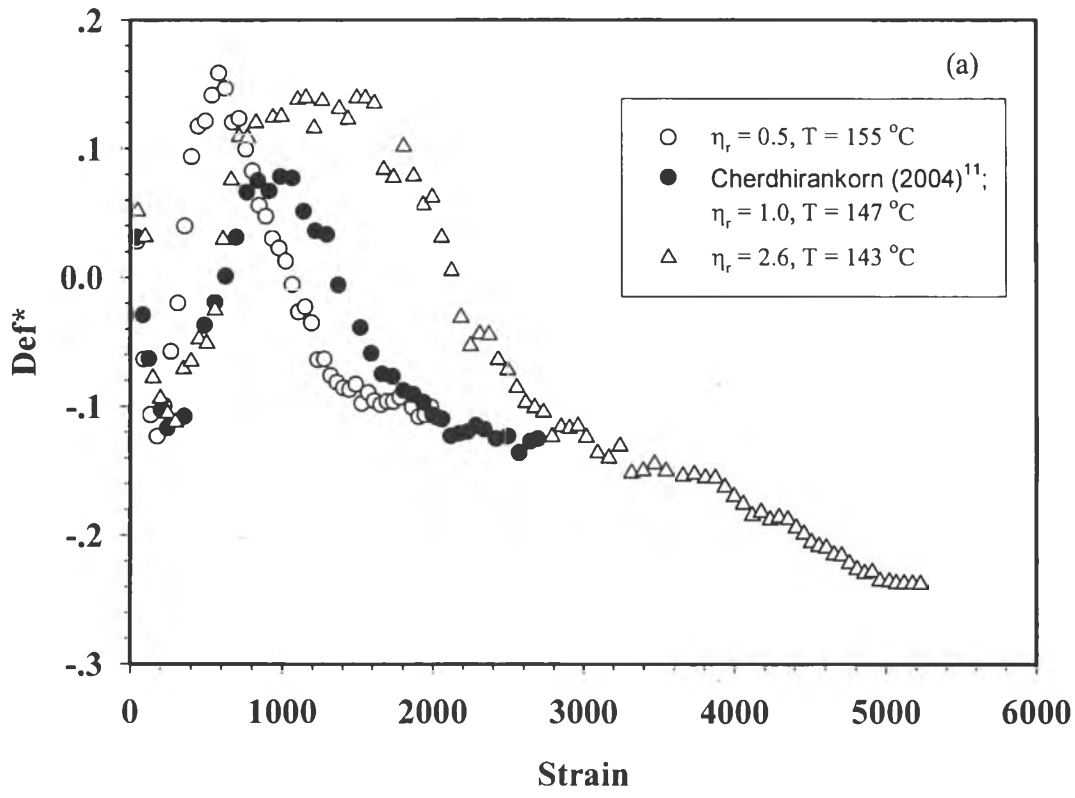

Figure 4a Def* vs. strain at various viscosity ratios, η_r, Ca =8 and $Wi_d \approx 0.30$: η_r = 0.5, $\dot{\gamma}$ = 0.63 s^{-1}, (○); η_r = 1.0, $\dot{\gamma}$ = 0.50 s^{-1}, (●); η_r = 2.6, $\dot{\gamma}$ = 0.40 s^{-1}, (△).

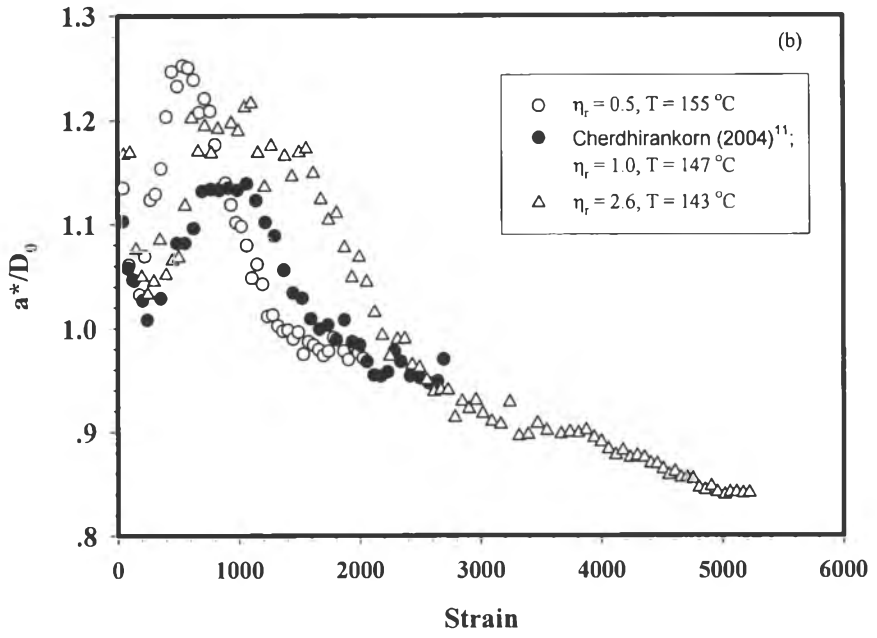

Figure 4b a^*/D_0 vs. strain at various viscosity ratios, η_r, Ca =8 and $Wi_d \approx 0.30$: η_r = 0.5, $\dot{\gamma}$ = 0.63 s^{-1}, (○); η_r = 1.0, $\dot{\gamma}$ = 0.50 s^{-1}, (●); η_r = 2.6, $\dot{\gamma}$ = 0.40 s^{-1}, (△).

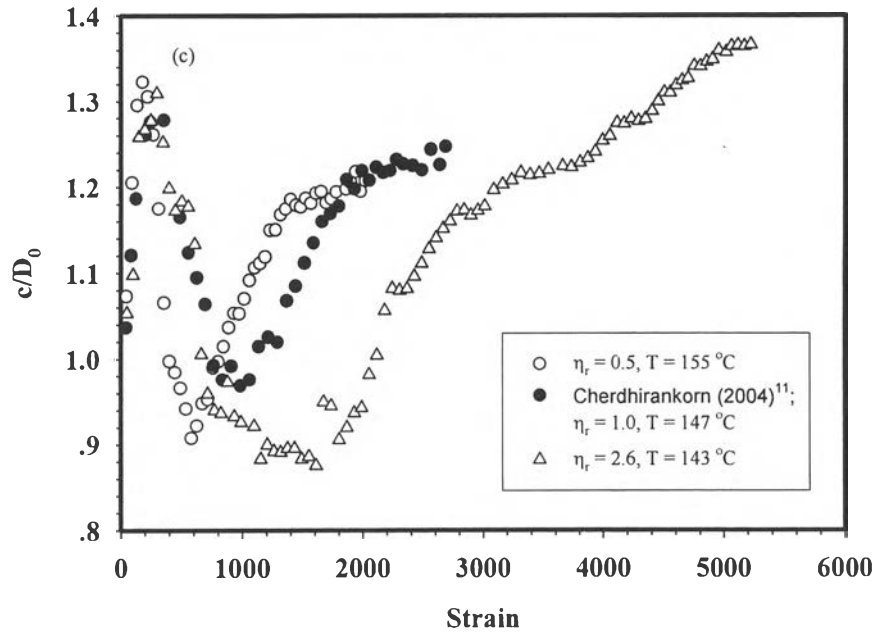

Figure 4c c/D_0 vs. strain at various viscosity ratios, η_r,Ca =8 and $Wi_d \approx 0.30$: η_r = 0.5, $\dot{\gamma}$ = 0.63 s^{-1}, (○); η_r = 1.0, $\dot{\gamma}$ = 0.50 s^{-1}, (●); η_r = 2.6, $\dot{\gamma}$ = 0.40 s^{-1}, (△).

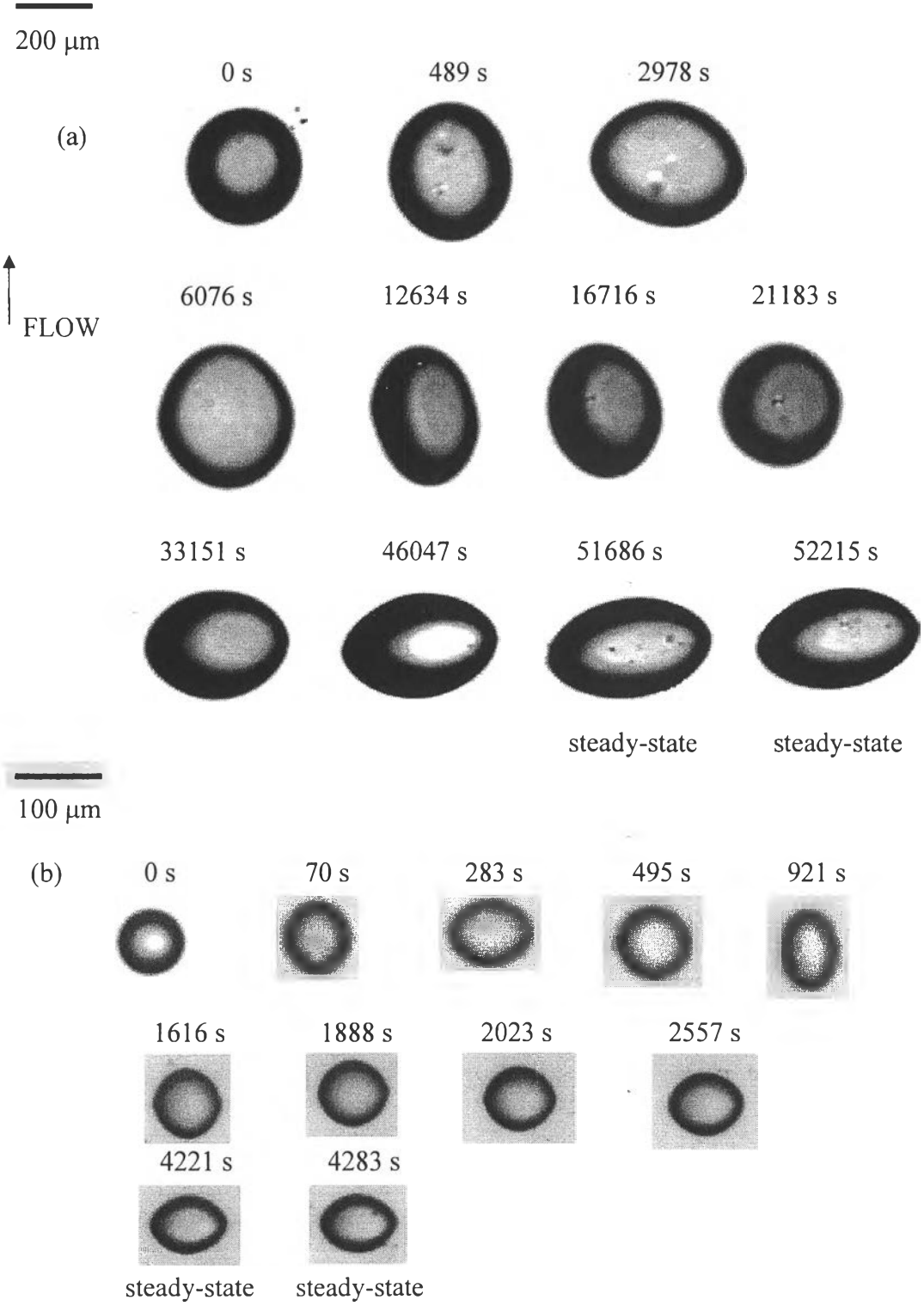

Figure 5 Sequence of images of deformed droplets after startup of a steady shear $Wi_d \approx 0.30$, Ca = 8: (a) system A, $\eta_r = 2.6$ at a rate of 0.1 s^{-1}, $D_0 = 289.7$ μm ; (b) system B, $\eta_r = 0.5$ at a rate of 0.63 s^{-1}, $D_0 = 72.2$ μm.

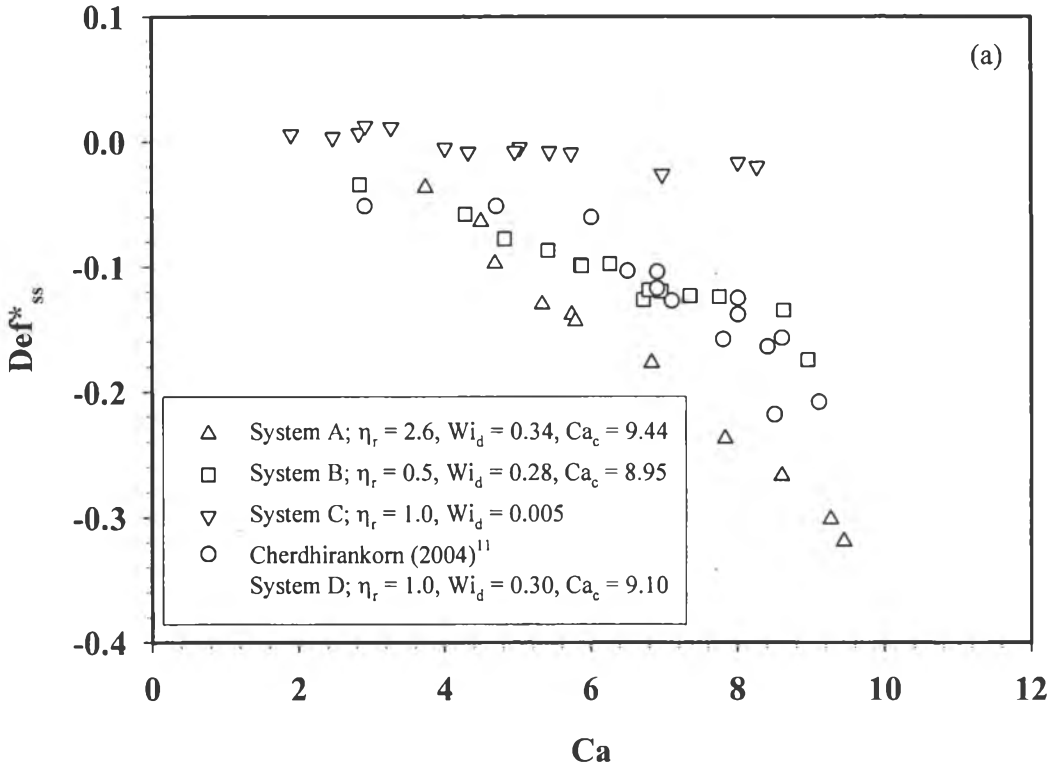

Figure 6a Steady-state deformation vs. Ca: $Wi_d \approx 0.30$: system A $\eta_r = 2.6$ at shear rate of 0.4 s^{-1}, (△); system D of Cherdhirankorn et al. (2004)[11] $\eta_r = 1.0$ at shear rate of 0.5 s^{-1}, (○); system B $\eta_r = 0.5$ at shear rate of 0.63 s^{-1}, (□); system C, $Wi_d = 0.005$, $\eta_r = 1.0$ at shear rate of 0.4 s^{-1}, (▽), Ca is varied by varying droplet size.

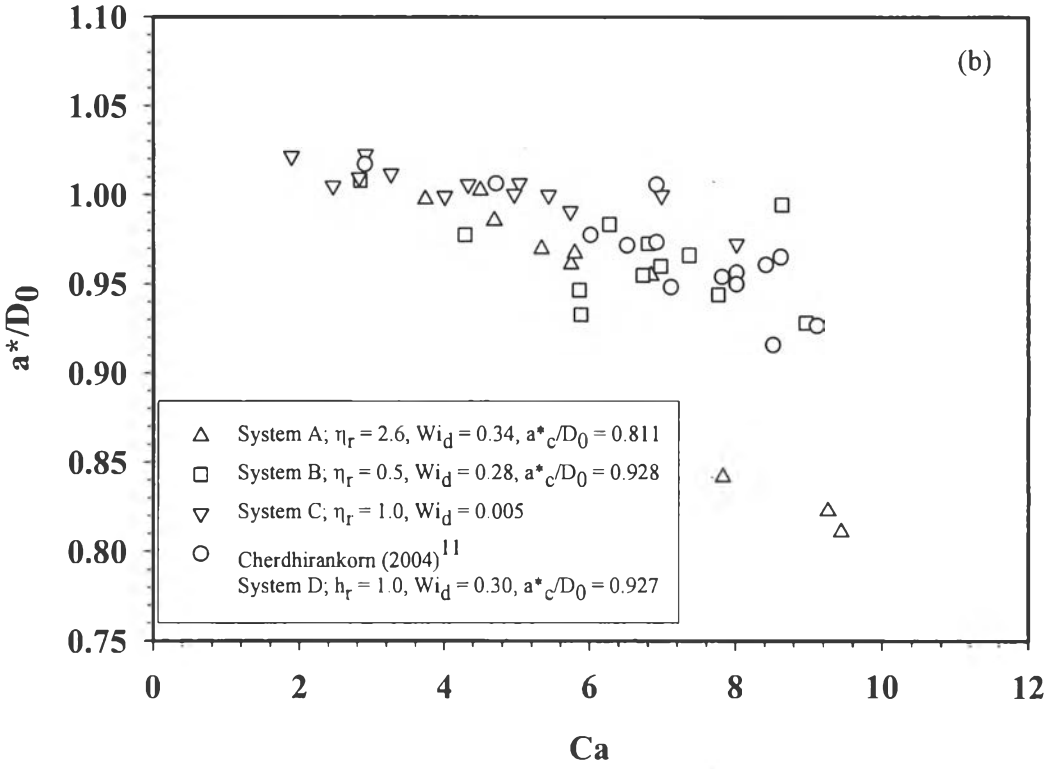

Figure 6b a^*/D_0 vs. Ca: $Wi_d \approx 0.30$: system A $\eta_r = 2.6$ at shear rate of 0.4 s^{-1}, (△); system D of Cherdhirankorn et al. (2004)[11] $\eta_r = 1.0$ at shear rate of 0.5 s^{-1}, (○); system B $\eta_r = 0.5$ at shear rate of 0.63 s^{-1}, (□); system C, $Wi_d = 0.005$, $\eta_r = 1.0$ at shear rate of 0.4 s^{-1}, (▽), Ca is varied by varying droplet size.

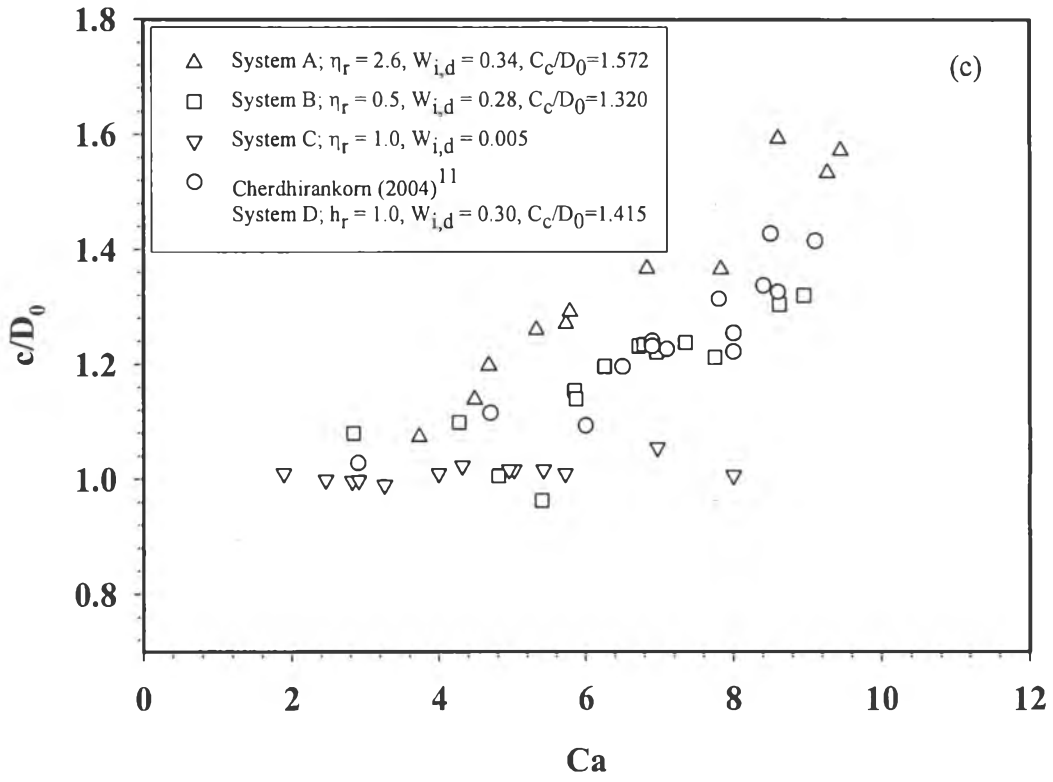

Figure 6c c/D_0 vs. Ca: $Wi_d \approx 0.30$: system A $\eta_r = 2.6$ at shear rate of 0.4 s^{-1}, (△); system D of Cherdhirankorn et al. (2004)[11] $\eta_r = 1.0$ at shear rate of 0.5 s^{-1}, (○); system B $\eta_r = 0.5$ at shear rate of 0.63 s^{-1}, (□); system C, $Wi_d = 0.005$, $\eta_r = 1.0$ at shear rate of 0.4 s^{-1}, (▽), Ca is varied by varying droplet size.

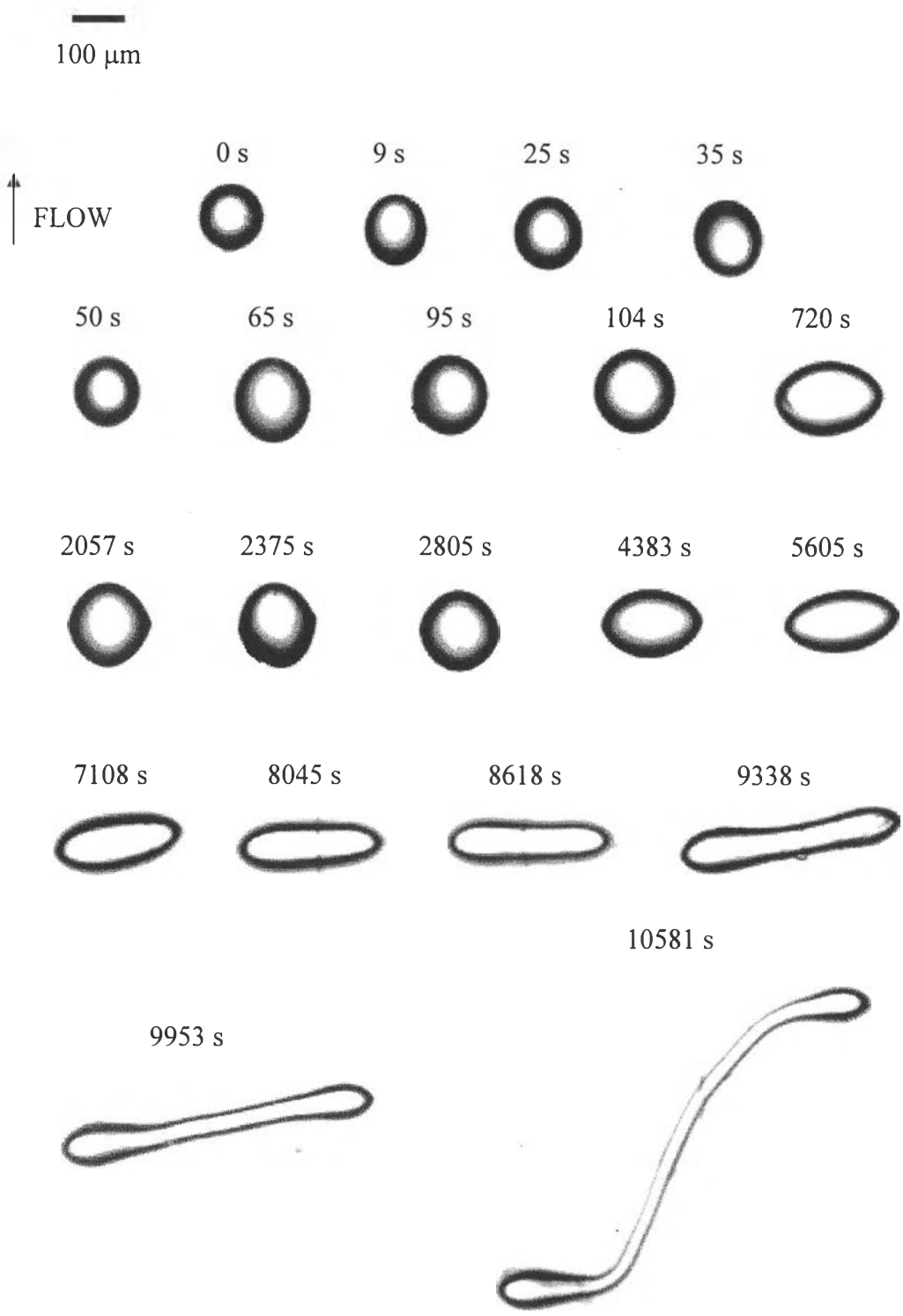

Figure 7 Sequence of images of droplet breakup of the system A at a shear rate of 0.4 s^{-1} , D_0 = 125 (±7) μm, Wi_d = 0.75 for η_r = 2.6, Ca = 11.

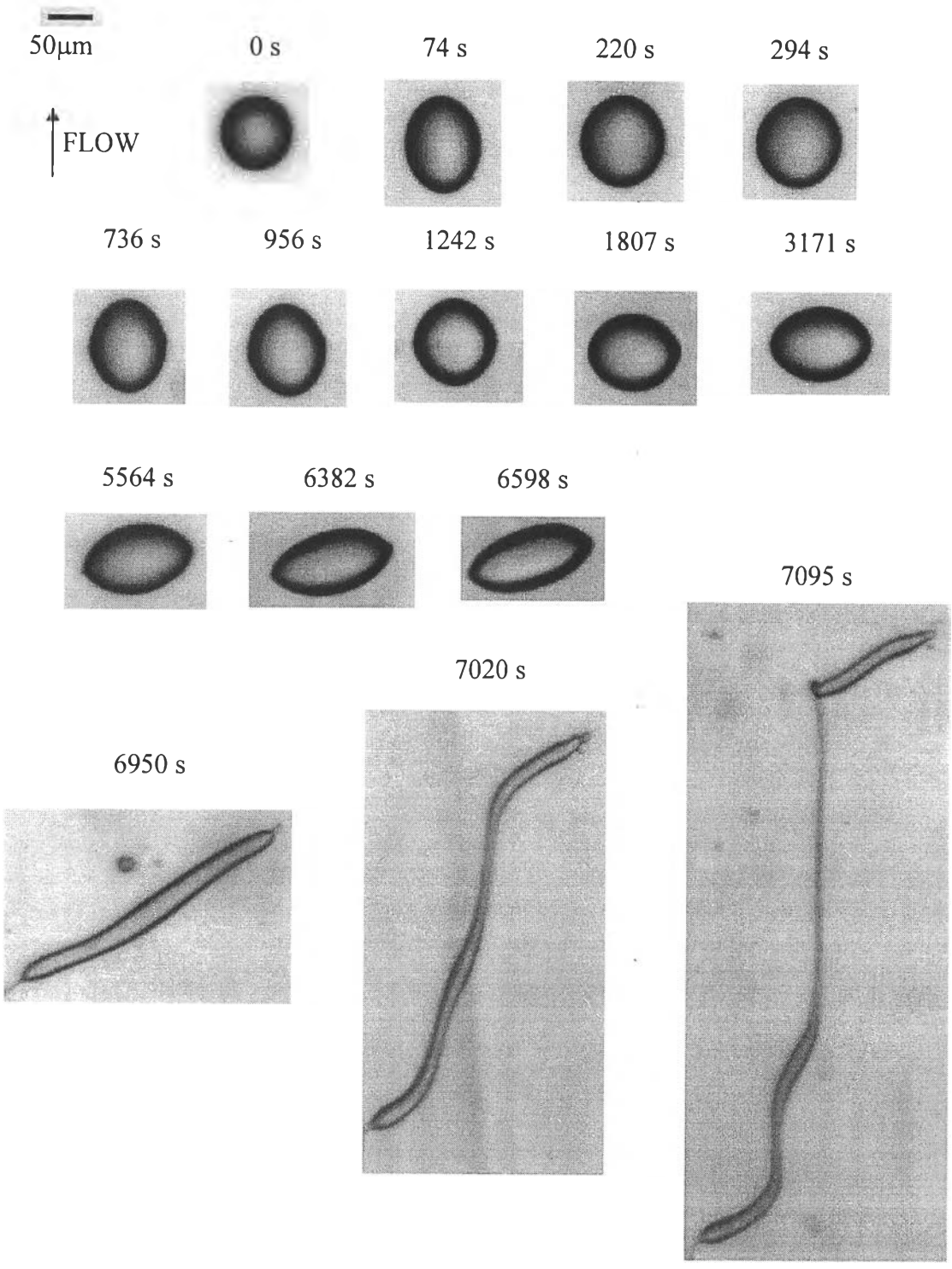

Figure 8 Sequence of images of droplet breakup of the system B at a shear rate of 0.63 s^{-1} , D_0 = 81.6 μm, Wi_d = 0.28 for η_r = 0.5, Ca = 9.5.

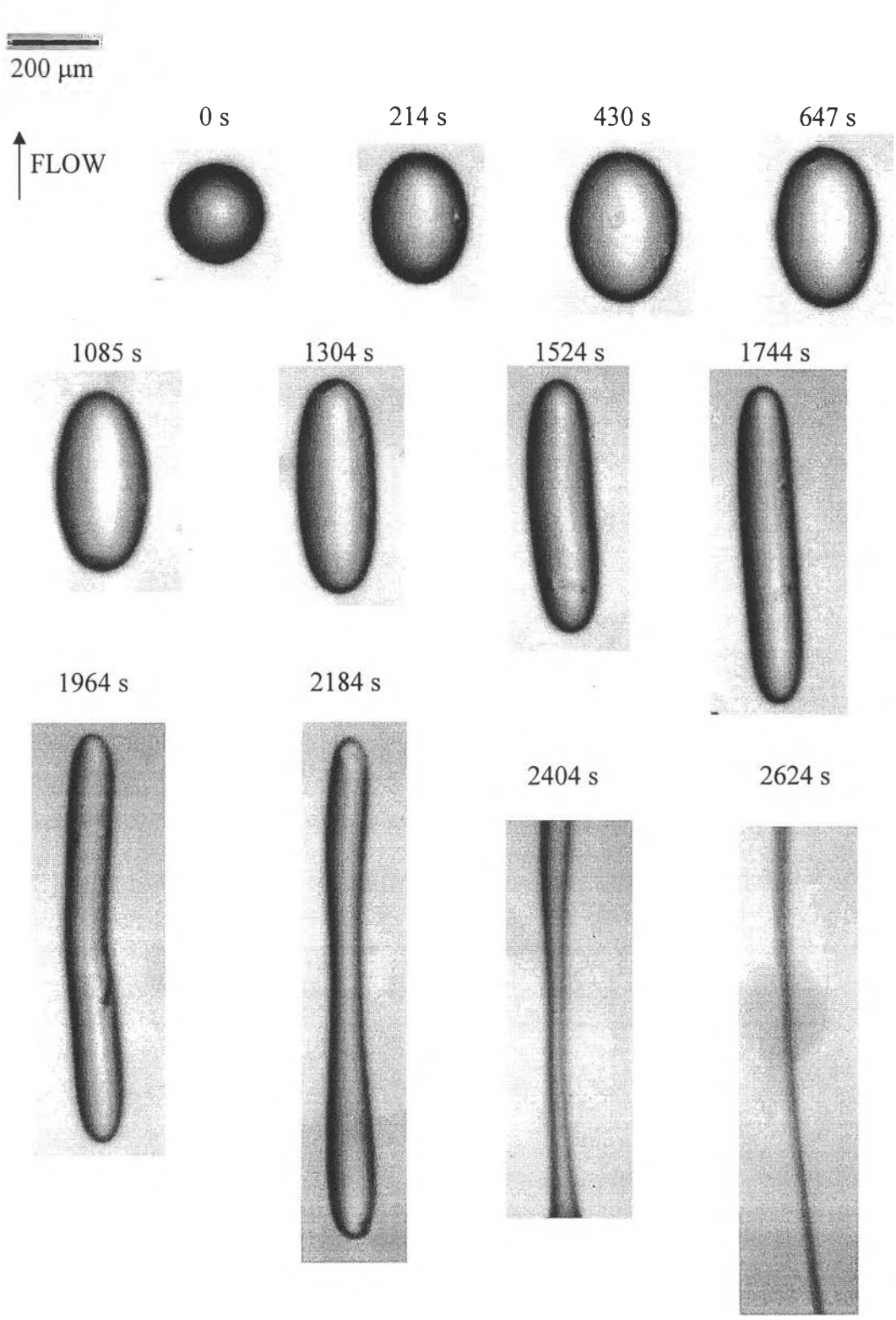

Figure 9 Sequence of images of droplet breakup of the system B at a shear rate of 0.20 s^{-1} , D_0 = 225.3 μm, Wi_d = 0.25 for η_r = 0.5, Ca = 9.5.